ACS APPLIED MATERIALS & INTERFACES

Research Article

www.acsami.org

Accelerated Blood Clearance Phenomenon Reduces the Passive Targeting of PEGylated Nanoparticles in Peripheral Arterial Disease

Hyung-Jun Im,[†,‡,#] Christopher G. England,[§,#] Liangzhu Feng,[∥] Stephen A. Graves,[§] Reinier Hernandez,[§] Robert J. Nickles,[§] Zhuang Liu,[∥] Dong Soo Lee,[‡] Steve Y. Cho,[†] and Weibo Cai*[,†,§,⊥]

[†]Department of Radiology, University of Wisconsin—Madison, Madison, Wisconsin 53705, United States

[‡]Department of Molecular Medicine and Biopharmaceutical Sciences, Department of Nuclear Medicine, Seoul National University, Seoul 110-744, Korea

[§]Department of Medical Physics, University of Wisconsin—Madison, Madison, Wisconsin 53705, United States

[∥]Jiangsu Key Laboratory for Carbon-Based Functional Materials & Devices Laboratory, Soochow University Suzhou, Jiangsu 215123, China

[⊥]University of Wisconsin Carbone Cancer Center, Madison, Wisconsin 53705, United States

Supporting Information

ABSTRACT: Peripheral arterial disease (PAD) is a leading global health concern. Due to limited imaging and therapeutic options, PAD and other ischemia-related diseases may benefit from the use of long circulating nanoparticles as imaging probes and/or drug delivery vehicles. Polyethylene glycol (PEG)-conjugated nanoparticles have shown shortened circulation half-lives *in vivo* when injected multiple times into a single subject. This phenomenon has become known as the accelerated blood clearance (ABC) effect. The phenomenon is of concern for clinical translation of nanomaterials as it limits the passive accumulation of nanoparticles in many diseases, yet it has not been evaluated using inorganic or organic−inorganic hybrid nanoparticles. Herein, we found that the ABC phenomenon was induced by reinjection of PEGylated long circulating organic−inorganic hybrid nanoparticles, which significantly reduced the passive targeting of ^{64}Cu-labeled PEGylated reduced graphene oxide−iron oxide nanoparticles (^{64}Cu-RGO-IONP-PEG) in a murine model of PAD. Positron emission tomography (PET) imaging was performed at 3, 10, and 17 days postsurgical induction of hindlimb ischemia. At day 3 postsurgery, the nanoparticles displayed a long circulation half-life with enhanced accumulation in the ischemic hindlimb. At days 10 and 17 postsurgery, reinjected mice displayed a short circulation half-life and lower accumulation of the nanoparticles in the ischemic hindlimb, in comparison to the naïve group. Also, reinjected mice showed significantly higher liver uptake than the naïve group, indicating that the nanoparticles experienced higher sequestration by the liver in the reinjected group. Furthermore, photoacoustic (PA) imaging and Prussian blue staining confirmed the enhanced accumulation of the nanoparticles in the liver tissue of reinjected mice. These findings validate the ABC phenomenon using long circulating organic−inorganic hybrid nanoparticles upon multiple administrations to the same animal, which may provide valuable insight into the future clinical applications of nanoparticles for imaging and treatment of PAD.

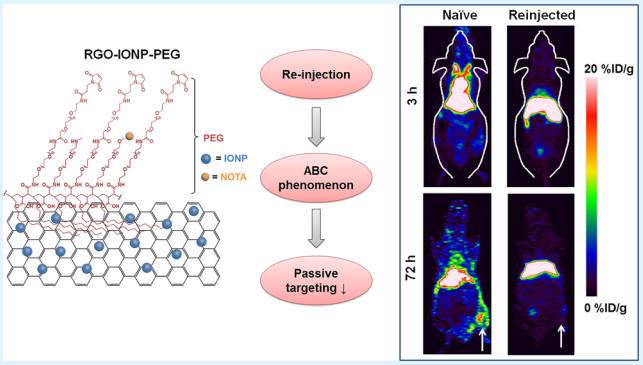

KEYWORDS: *accelerated blood clearance (ABC), peripheral arterial disease, reduced graphene oxide (RGO), iron oxide nanoparticle (IONP), anti-PEG antibody, hindlimb ischemia, positron emission tomography (PET), photoacoustic imaging*

INTRODUCTION

Peripheral arterial disease (PAD) results from the atherosclerotic stenosis of the peripheral arteries, especially in the lower extremities, and has become one of the major health concerns in elderly patients as it affects more than 200 million worldwide.[1,2] The restricted supply of oxygenated blood to the peripheral tissues results in intermittent claudication, slower wound healing, and possible gangrene in severe cases.[3] Critical limb ischemia (CLI) is the most severe form of PAD and is the leading cause of limb amputation worldwide.[4] Current treatment options for CLI include peripheral artery bypass surgery, proangiogenic growth factor therapy, and antiplatelet medications.[5] While surgical intervention is most effective, bypass surgery has been linked to several adverse effects, including heart attack, stroke, and infection. It has been shown that revascularization surgery works for only ∼40% of patients with CLI, which is why many patients rely upon other treatment options.[6] Proangiogenic growth factor (PGF)

Received: May 16, 2016
Accepted: June 24, 2016
Published: June 24, 2016

DOI: 10.1021/acsami.6b05840
ACS Appl. Mater. Interfaces 2016, 8, 17955−17963

therapy has been proposed to enhance the microvascular circulation,[7,8] yet low delivery efficiency and systemic off-target toxicites have effectively hampered the benefits of PGF treatment.[5] Additionally, some nonaspirin antiplatelet therapies (e.g., clopidogrel and ticlopidine) have reduced cardiovascular events in patients with PAD; yet these drugs fail to elicit symptomatic improvement in patients with intermittent claudication.[5,9] For these reasons, nanoparticle-based proangiogenic gene or growth factor delivery provides an alternative method to overcome the limitations of traditional treatment modalities. In particular, preclinical investigation of nanoparticle-based growth factor treatment showed significant improvement of the perfusion in a PAD model.[10]

We recently developed a long circulating organic−inorganic hybrid nanoparticle by coating two layers of polyethylene glycol (PEG) onto reduced graphene oxide iron oxide nanoparticles (RGO-IONP-PEG). RGO-IONP-PEG displays excellent theranostic properties which may be suitable for PAD imaging and therapy. The low perfusion rate found in PAD requires that successful imaging or therapeutic agents display long blood circulation times with high passive targeting capabilities. Previously, RGO-IONP-PEG was shown to display a long circulation half-life and excellent passive targeting efficiency in a murine tumor model.[11] In addition, RGO-IONP-PEG can load and deliver large drug payloads to diseased tissues, further proving that this nanoparticle may be a prime candidate for imaging-guided drug delivery in PAD.[12]

Accelerated blood clearance (ABC) phenomenon refers to the significantly decreased circulation half-life displayed by PEGylated nanomaterials when repeatedly injected *in vivo*.[13] The phenomenon was initially observed with PEGylated liposome,[14] yet has been reproduced using several nanoplatforms, including micelles[15] and PLGA nanoparticles.[16] This phenomenon is thought to be a result of increased splenic production of anti-PEG IgM.[17,18] While it has been investigated with lipid- or polymer-based nanoparticles, there are no reports evaluating the ABC phenomenon using inorganic or organic−inorganic hybrid nanoparticles.

In this work, we hypothesized that reinjection of PEGylated RGO-IONP will induce the ABC phenomenon, resulting in a significant decrease in the circulation half-life and passive targeting capabilities of these nanoparticles. By comparing the reinjected group with mice that were not reinjected (naïve), we verified that the circulation half-life and passive accumulation of RGO-IONP-PEG in the ischemic tissues was significantly decreased. A murine model of PAD was produced by ligation and cutting of the femoral artery. At 3, 10, and 17 days postsurgery, mice were scanned for up to 72 h with PET after receiving an intravenous injection of ^{64}Cu-RGO-IONP-PEG. As the ischemic hindlimb heals postsurgery, vasculature normalization will result in decreased nanoparticle accumulation as the enhanced permeability and retention (EPR) effect is diminished.[19] Two different animal groups were utilized, including a naïve group in which different mice were used at each time point (Day 3, 10, and 17 postsurgery) and a reinjected group with mice that were serially injected at Days 3, 10, and 17 postsurgery. At Day 10 and 17 postsurgery, the reinjected group showed faster blood clearance and higher liver uptake of the nanoparticle, as compared to the naïve group, validating the effects of the ABC phenomenon. Also, decreased nanoparticle accumulation in the ischemic hindlimb of reinjected mice indicated that passive targeting was effectively reduced by an ABC effect. The phenomenon was considered to be mediated by anti-PEG IgM and based on ELISA results showed that anti-PEG IgM was present at 7 and 14 days after injection of the nanoparticles. Furthermore, we confirmed that the nanoparticles were cleared to the liver, using photoacoustic imaging and histologic examination of liver tissue.

EXPERIMENTAL SECTION

RGO-IONP-PEG Production and PEGylation. The syntheses of nanoparticles (RGO-IONP-PEG) were previously provided.[20] Synthesis of the nanoparticles was accomplished using a modified version of the Hammer method. As PEGylation improves the overall circulation of nanoparticles, 10 mg of poly(maleicanhydride-*alt*-1-octadecene) (PEG) (Sigma-Aldrich, Madison, WI, USA) was used to functionalize RGO-IONP (1 mg). An additional layer of PEG was conjugated to increase circulation time. Also NOTA was conjugated for radiolabeling. p-SCN-Bn-NOTA (NOTA, Macrocyclics, Inc., Dallas, TX, USA) was conjugated to the nanoparticles with 1:4 molar ratio of nanoparticle:chelator. NOTA was conjugated to the nanoparticles post-PEGylation. NOTA-RGO-IONP characterization was reported in previous work.[11]

Murine Model of Hindlimb Ischemia. All animal studies were conducted under a protocol approved by the University of Wisconsin Institutional Animal Care and Use Committee. Using six-week-old female BALB/c mice (Harlan, Indianapolis, IN), the right unilateral hindlimb ischemia was produced as previously described.[21] Briefly, an incision at the midabdominal level was made to expose the femoral triangle, after the mice were anesthetized with 2% isoflurane. Using an intraoperative microscope, the right femoral artery was isolated from the femoral vein and nerve, and the artery was sutured in two locations and cut in-between to disrupt the blood flow using nylon sutures (6/0; ARO Surgical Corp., Newport Beach, CA).

Laser Doppler Perfusion Imaging. Imaging of both hindlimbs was performed before and directly after surgical induction of ischemia using the high-resolution moorLDI2-HR laser Doppler imager (Moor Instruments, DE, USA).

Radiolabeling of RGO-IONP-PEG. ^{64}Cu production was previously described.[22] Briefly, $^{64}CuCl_2$ was mixed with 200 μL of RGO-IONP-PEG and incubated for 30 min (37 °C; 550 rpm). A PD-10 column was used to purify the sample from nonlabeled isotope.

Positron Emission Tomography Imaging and Quantitative Analyses. The Inveon microPET/microCT rodent scanner (Siemens Medical Solutions USA, Inc.) was used for imaging after mice were injected with 8−10 MBq of radiolabeled nanoparticle. PET image acquisition, reconstruction, decay correction, and region-of-interest (ROI) analysis were carried out as previously described.[23] Quantitative PET data were presented as a percent of injected dose per gram of tissue (% ID/g) with 3−4 mice per group.

Ex Vivo Biodistribution. Biodistribution of the tracer was used to confirm results from PET imaging. After mice were euthanized, we collected the blood, major organs/tissues, and ischemic/nonischemic muscle. γ Radiation in the samples was measured in a Wizard 2 Automatic Gamma Counter from PerkinElmer, and the values were recorded in % ID/g with 3−4 mice per group.

Histological Staining of Tissues. Histological sectioning and hematoxylin and eosin (H&E) staining of tissues were performed by the Experimental Pathology core facility at the Carbone Cancer Center. Tissues were sliced at 5−7 μm, and the Iron Staining Kit from Sigma-Aldrich (St. Louis, MO, USA) was used to stain iron in the tissue sections. Tissue sections were incubated in cold CH_3OH for 10−15 min before incubation with a solution of 1 part $K_4[Fe(CN)_6]\cdot 3H_2O$, and 1 part HCl was applied to the slides for 8−10 min before washing with cold tap H_2O. After the slides were dried and coverslipped, the slides were imaged using bright-field microscopy.

Ultrasound and Photoacoustic Imaging Techniques. Ultrasonography and photoacoustic imaging were accomplished using the Vevo LAZR System from VisualSonics (Toronto, Canada). Photoacoustic imaging was performed in the liver before and 12 h after injection of ^{64}Cu-RGO-IONP-PEG using an 808 nm laser with a depth penetration focal point of 10 mm.

DOI: 10.1021/acsami.6b05840
ACS Appl. Mater. Interfaces 2016, 8, 17955−17963

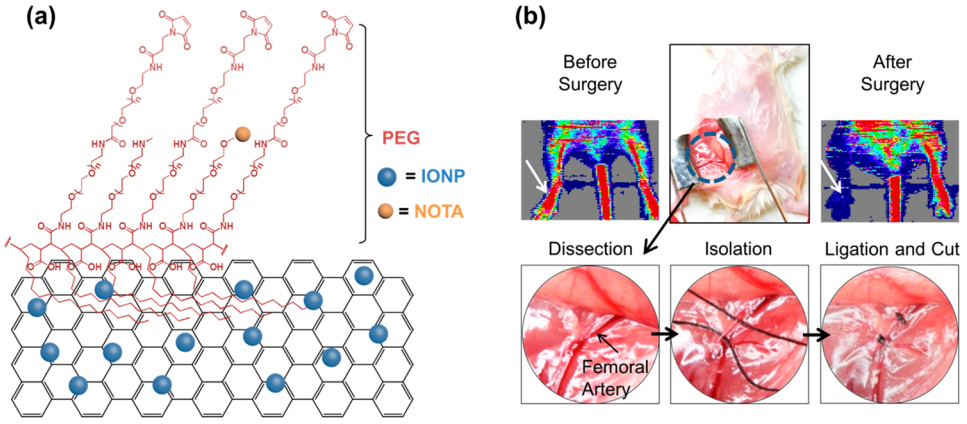

Figure 1. PEGylated reduced graphene oxide−iron oxide nanoparticles (RGO-IONP-PEG) for imaging of peripheral arterial disease in a mouse model of hindlimb ischemia. (a) Schematic drawing of the RGO-IONP-PEG nanoparticle. On a sheet of reduced graphene oxide (RGO), iron oxide nanoparticles (IONPs) are conjugated (RGO-IONP). RGO-IONP was functionalized with NOTA and two layers of PEG. (b) The murine model of hindlimb ischemia is a representative model of human PAD. A midabdominal incision was made, and the adjacent fat tissue and fascia were dissected to visualize the femoral artery for isolation, ligation, and cutting to produce the ischemic hindlimb. The white arrow indicates the surgical hindlimb in the Doppler ultrasound imaging. Doppler ultrasound imaging revealed a significantly decreased red signal in the ischemic hindlimb, indicating decreased blood flow and confirming the successful generation of the PAD model.

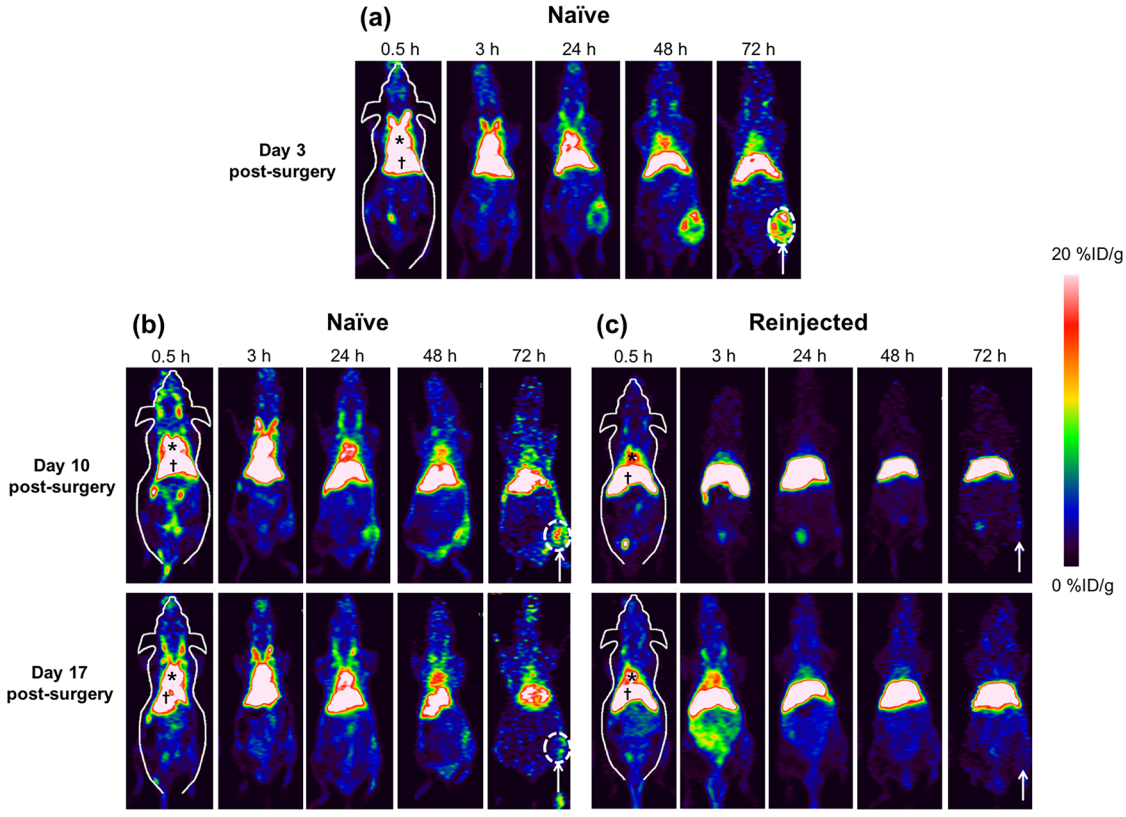

Figure 2. PET imaging of ^{64}Cu-RGO-IONP-PEG in mice. PET imaging was performed at 3, 10, and 17 days postsurgical induction of hindlimb ischemia in mice. Images were acquired from 30 min to 72 h after nanoparticle injection. (a) At Day 3 postsurgery, high nanoparticle accumulation in circulation and the ischemic hindlimb was found. (b, c) At Day 10 and 17 postsurgery, the naïve group showed prolonged blood pool uptake, yet the reinjected group showed significantly lower uptake in the blood pool. Nanoparticle uptake in the ischemic hindlimb of reinjected mice was lower than that of the naïve group at Day 10 and 17 postsurgery. The region of interest used for quantitative analysis is outlined in white for the naïve group. * = blood pool, † = liver, white arrow = ischemic hindlimb.

Anti-PEG IgM Enzyme-Linked Immunosorbent Assay (ELISA). Anti-PEG IgM was detected using a mouse anti-PEG IgM ELISA kit (Life diagnostics, West Chester, PA, USA). Mouse serum was collected before injection of nanoparticles and at Day 7 and 14 postinjection of ^{64}Cu-RGO-IONP-PEG (56.1 μg per mouse). Mouse serum was diluted 25-fold and dispensed into the wells. After incubation for 1 h at 100−150 rpm at room temperature, well contents were aspirated, and the wells were washed five times with 1X wash solution. Next, 100 mL of diluted horseradish peroxidase conjugate was added into each well. The wells were incubated for 30 min at room temperature with shaking at 100−150 rpm before washing five times. The 3,3′,5,5′-tetramethylbenzidine (TMB) reagent was added

DOI: 10.1021/acsami.6b05840
ACS Appl. Mater. Interfaces 2016, 8, 17955−17963

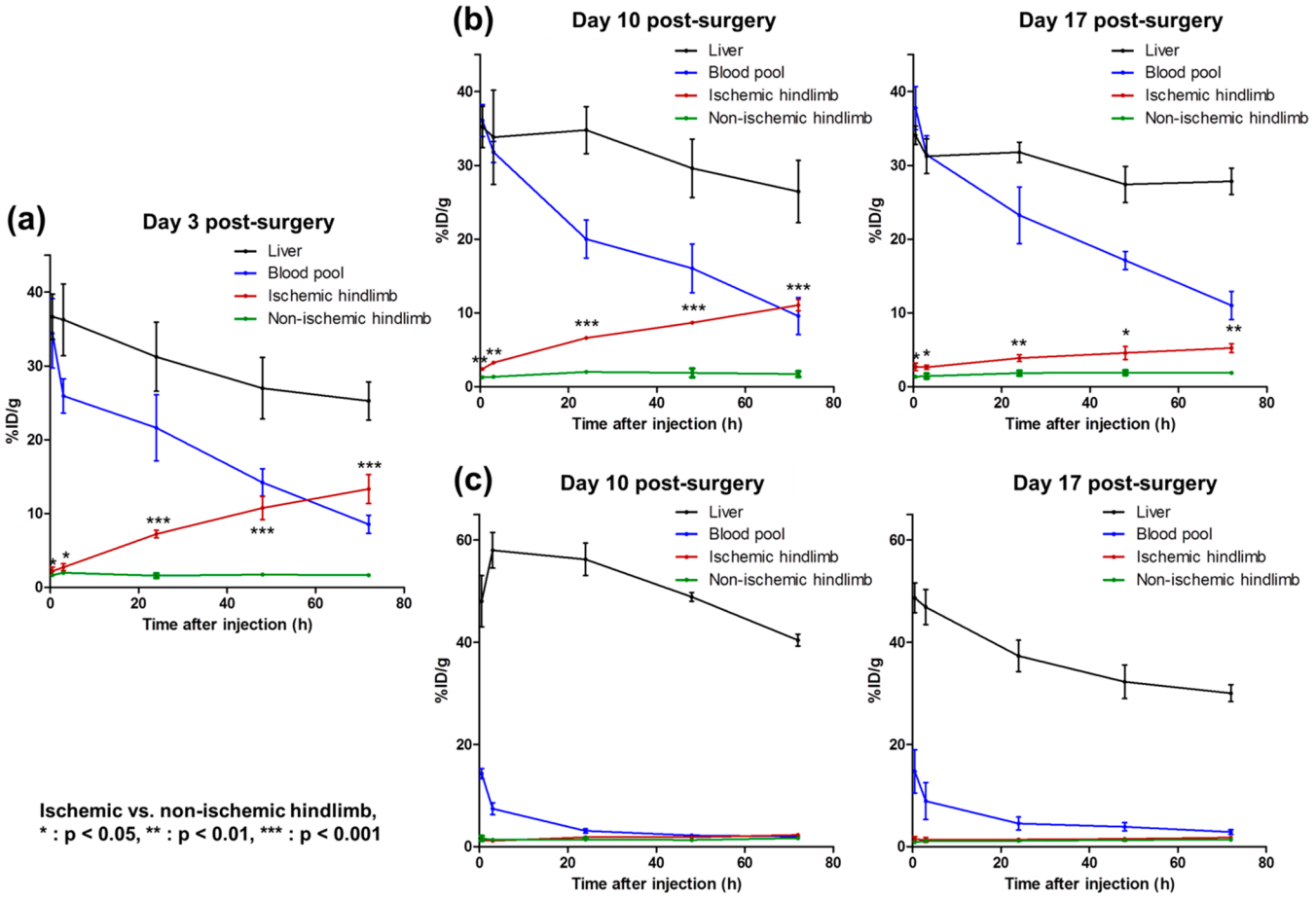

Figure 3. Pharmacokinetics of ^{64}Cu-RGO-IONP-PEG in hindlimb ischemia-induced mice. (a) At Day 3 postsurgery, the nanoparticle displayed excellent stability in the blood pool, with significantly higher uptake in the ischemic hindlimb than the nonischemic hindlimb. (b) The long circulation half-life of ^{64}Cu-RGO-IONP-PEG was found in the naïve group at Day 10 and 17 postsurgery. Also, nanoparticle accumulation in the ischemic hindlimb remained significantly higher than that of the nonischemic hindlimb, although the values were lower than Day 3 postsurgery. (c) Decreased circulation half-life and increased liver sequestration were found in the reinjected group. Nanoparticle localization in the ischemic hindlimb was similar to that of the nonischemic hindlimb. Each value represents the mean ± SD (n = 4).

into each well and incubated at room temperature for 20 min. Finally, 100 mL of Stop Solution (1 N HCl) was added to stop the reaction. The optical density was measured at 450 nm with a microtiter plate reader (BioTek, Winooski, VT, USA).

Statistical Tests. All values were presented as mean ± standard deviation. Student t-test was performed to assess the difference between the mean values from two groups, and a p value less than 0.05 was used to define statistical significance.

RESULTS AND DISCUSSION

Synthesis of RGO-IONP-PEG. RGO-IONP-PEG was synthesized according to the procedures previously described.[20] Two layers of PEG were added to the surface of the nanoparticles to extend their circulation time. A well-known chelator for ^{64}Cu labeling, known as NOTA (1,4,7-triazacyclononane-triacetic acid), was conjugated for *in vivo* PET imaging (Figure 1a). The nanoparticles were characterized to determine the morphology, diameter, and surface charge (Figure S1). The morphology and size of the nanoparticles were examined by atomic force microscopy (AFM) and dynamic light scattering (DLS), respectively. The hydrodynamic diameter of the nanoplatform was found to be 92.68 ± 33.3 nm with a polydispersity index (PDI) of 0.16. Also, the UV−visible spectrum was consistent with previous data, further verifying the identity of the nanoparticles.[20] In addition, the zeta potential was calculated as −10.2 ± 0.9 mV. Previously, we have shown that RGO-IONPs display high serum stability with over 90% of radiolabeled nanoparticles remaining stable at 40 h.[11]

RGO-IONP-PEG displays excellent theranostic properties, making it suitable for both molecular imaging and therapy of many diseases, including PAD. The long circulation half-life and high passive targeting capabilities of RGO-IONP-PEG are essential for ischemic-related diseases, as the low perfusion rate can effectively limit the access of nanoparticles to the ischemic tissues. In addition to its excellent theranostic properties, ^{64}Cu-RGO-IONP-PEG can function as a triple modality imaging probe for PET, MR, and photoacoustic imaging, with each imaging modality providing essential information regarding PAD progression and therapeutic response. While PET provides high sensitivity and quantifiability needed for grading the disease severity, the high spatial resolution of MR can compensate for the low resolution of PET, making it possible to better determine the spatiotemporal localization of the disease.[20] While image-guided procedures are difficult using PET and MRI, photoacoustic (PA) imaging provides new avenues for potential image-guided therapies. Lastly, previous studies have shown that RGO-IONP-PEG can effectively load considerable drug payloads for delivery to numerous diseases.[24]

DOI: 10.1021/acsami.6b05840
ACS Appl. Mater. Interfaces 2016, 8, 17955−17963

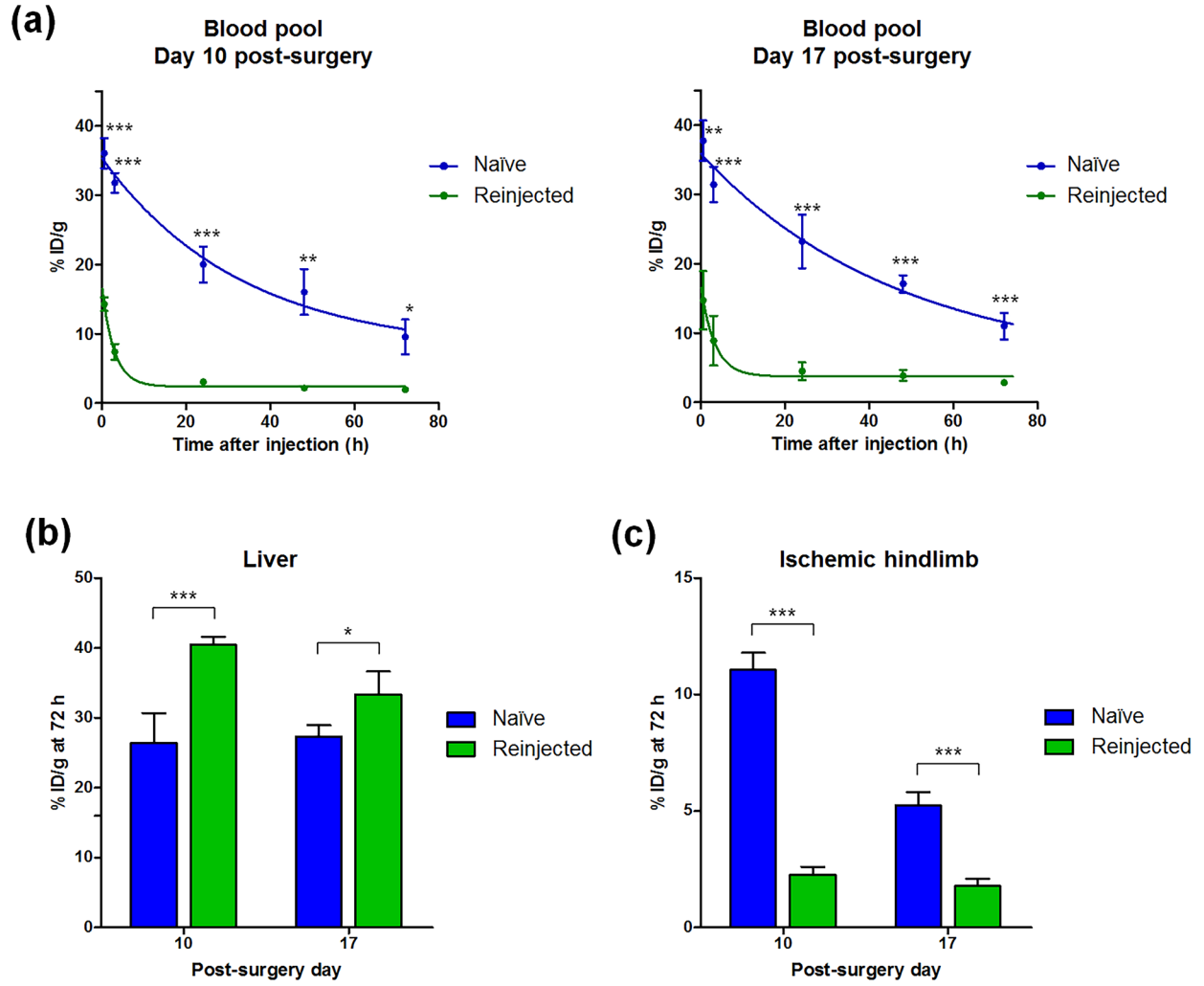

Figure 4. Comparison of nanoparticle pharmacokinetics in the blood pool, liver, and ischemic hindlimb between naïve and reinjected mice. (a) Blood pool activity in the naïve group was consistently higher than that of the reinjected group. (b) Liver uptake of the nanoparticle at 72 h after injection was compared between the naïve and reinjected group. Liver uptake was higher in the reinjected group than the naïve group at Day 10 and 17 postsurgery. (c) Nanoparticle uptake in the ischemic hindlimb at 72 h postinjection was higher in the naïve group than the reinjected group at Day 10 and 17. Each value represents the mean ± SD (n = 4). Naïve vs Reinjected, *: $p < 0.05$, **: $p < 0.01$, ***: $p < 0.001$.

Production of Murine Model of Hindlimb Ischemia. Hindlimb ischemia was induced by ligation and cutting of the femoral artery in mice.[25] A midabdominal incision was made after induction of anesthesia using isoflurane (Figure 1b). After dissection of adjacent fat tissue and fascia, the femoral artery, vein, and nerve were visualized. The femoral artery was isolated and ligated after separation from the femoral vein and nerve. Lastly, the femoral artery was cut to induce ischemia in the hindlimb. Laser Doppler images showed significantly decreased blood flow in the surgical hindlimb, which confirmed the successful creation of the ischemic model (Figure 1b). After surgical induction of ischemia, the hindlimb gradually heals over time with vasculature normalizing between 20 and 30 days postsurgery.[21] As the hindlimb heals and the vascularization normalizes, the EPR effect will decrease, resulting in less nanoparticle accumulation at later times postsurgery.[19] While the EPR effect has been extensively documented in cancer, activation and mobilization of endothelial cells in ischemic tissues also results in leaky vasculature, which is a key attributor to the EPR effect in solid tumors.[26]

PET Imaging and Analysis. At 3, 10, and 17 days postsurgical induction of hindlimb ischemia, mice were injected (naïve) or reinjected with ^{64}Cu-RGO-IONP-PEG, and PET imaging was performed at different time points up to 72 h postinjection. At Day 3, all mice received an injection of ^{64}Cu-RGO-IONP-PEG for the first time. At Day 10 and Day 17, noninjected mice were used for the naïve group, while the same mice were used for the reinjected group previously injected on Day 3 postsurgery. At Day 3 postsurgery, PET imaging revealed high blood pool uptake through 48 h postinjection. The nanoparticle effectively accumulated in the ischemic hindlimb by 24 h postinjection. At Days 10 and 17 postsurgery, the pharmacokinetic profile of ^{64}Cu-RGO-IONP-PEG was significantly different between the naïve and reinjected mice, with the naïve group showing prolonged blood pool uptake, while the nanoparticles were rapidly cleared from the circulation of reinjected mice. Also, ischemic hindlimb uptake of ^{64}Cu-RGO-IONP-PEG was lower in reinjected mice (Figure 2).

Quantitative analysis using region of interest (ROI) on organs was used to quantify the PET imaging data. In the naïve group, high % ID/g in blood pool validated the long circulation half-life of RGO-IONP-PEG. Also, nanoparticle localization in the ischemic hindlimb was significantly higher than that of nonischemic hindlimb at all time points. The highest uptake of

DOI: 10.1021/acsami.6b05840
ACS Appl. Mater. Interfaces 2016, 8, 17955−17963

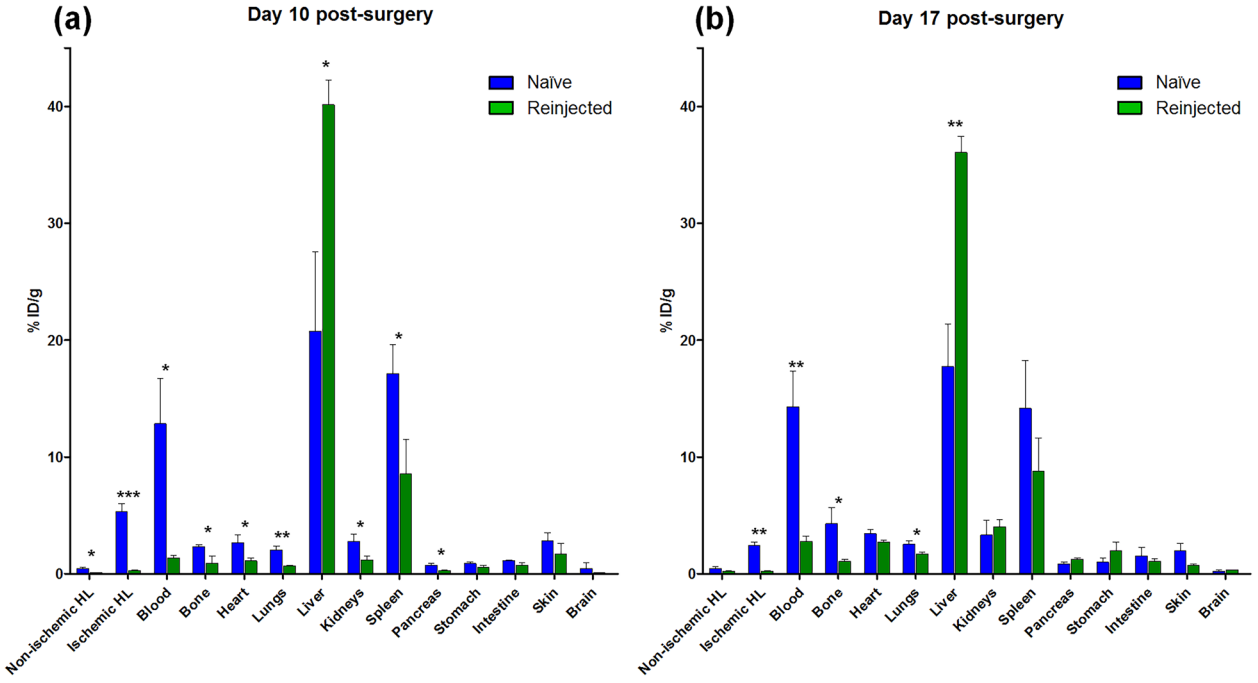

Figure 5. Comparison of *ex vivo* biodistribution between the naïve and reinjected group at (a) Day 10 and (b) Day 17. Each value represents the mean ± SD (n = 4). HL: hindlimb, Naïve vs Reinjected, *: $p < 0.05$, **: $p < 0.01$, ***: $p < 0.001$.

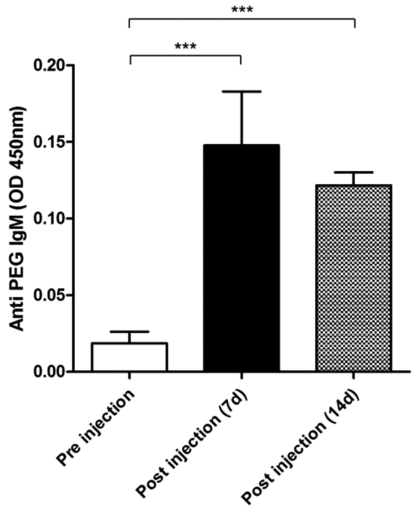

Figure 6. ELISA for anti-PEG IgM antibody. At 7 and 14 days after injection of ^{64}Cu-RGO-IONP-PEG, the presence of anti-PEG IgM was detected in mouse serum by ELISA. Each value represents the mean ± SD (n = 4).

nanoparticles in the ischemic hindlimb was found at Day 3 postsurgery (13.3 ± 1.9% ID/g; n = 4), which slowly diminished by Day 10 (11.1 ± 0.8% ID/g; n = 4) and Day 17 postsurgery (2.3 ± 0.3% ID/g; n = 4). From these data, we concluded the capability of effective passive targeting of the nanoparticle (Figure 3a,b). The reinjected group showed lower nanoparticle accumulation in the blood pool and higher accumulation in the liver than the naïve group. Also, there was no statistically significant difference in the localization of nanoparticles between the nonischemic and ischemic hindlimb in reinjected mice at Day 10 or Day 17 postsurgery (Figure 3c). Quantitative data of ^{64}Cu-RGO-IONP-PEG accumulation to the organs were determined (Tables S1−3).

Further quantitative analysis was performed using the % ID/g values of each organ. Activity in the blood pool activities was significantly higher in the naïve group at Day 10 and 17 postsurgery in comparison to the reinjected group. Nanoparticle clearance from the blood pool was faster in reinjected mice than naïve mice with circulation half-lives of 22.9 h (naïve group) and 2.0 h (reinjected group) at Day 10 postsurgery and 35.6 h (naïve group) and 2.3 h (reinjected group) at Day 17 postsurgery (Figure 4a). At 72 h postinjection of nanoparticles, the liver uptake of nanoparticles in the reinjected group was significantly higher than that of the naïve group at Day 10 (40.4 ± 1.2 vs 26.4 ± 4.2% ID/g; n = 4) and Day 17 (33.4 ± 3.2 vs 27.3 ± 1.6% ID/g; n = 4) postsurgery (Figure 4b). Meanwhile, nanoparticle accumulation in the ischemic hindlimb was significantly lower in the reinjected group than the naïve group with values of 2.3 ± 0.3 vs 11.1 ± 0.8% ID/g at Day 10 and 1.8 ± 0.3 vs 5.2 ± 0.6% ID/g at Day 17, respectively (n = 4; Figure 4c).

Multiple factors can affect the magnitude of the ABC phenomenon, with the prominent factor being the time interval between the injection and reinjection of PEGylated materials. Previously, the ABC effect was shown to be most prominent when PEGylated nanomaterials were injected and reinjected in rats within 7 days.[16] While this study utilized mice instead of rats, the seven day interval was still employed. Also, the structure and chemical composition of the nanocarriers may impact the magnitude of the ABC effect.[17,27] It was also shown that the ABC phenomenon occurs with cross-administration of different nanocarriers, and the degree of the ABC effect varied between different nanoparticle combinations.[27] However, there has been no study using inorganic or organic−inorganic hybrid nanoparticles to investigate the ABC phenomenon. In this study, PET imaging and quantitative analysis clearly verified that the ABC phenomenon was induced by reinjection of the PEGylated organic−inorganic hybrid nanoparticles (i.e., RGO-IONP-PEG).

DOI: 10.1021/acsami.6b05840
ACS Appl. Mater. Interfaces 2016, 8, 17955−17963

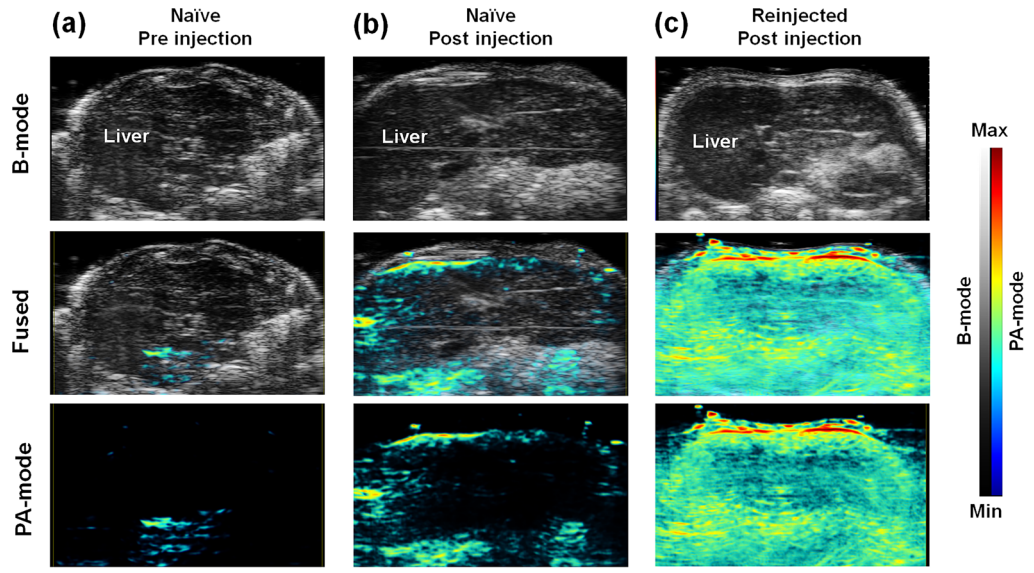

Figure 7. Photoacoustic imaging confirms the liver uptake of RGO-IONP-PEG. Ultrasound imaging (B-mode), which was utilized for anatomical information, and photoacoustic imaging (PA-mode) were obtained simultaneously. Increased PA signal validated the existence of nanoparticles in the liver. (a) PA signal was low in the naïve group before injection. (b, c) The PA signal was enhanced in both naïve and reinjected mice at 72 h postinjection of the nanoparticles. The reinjected group showed higher PA signal in the liver than the naïve group. B-mode: Brightness mode, PA-mode: Photoacoustic mode.

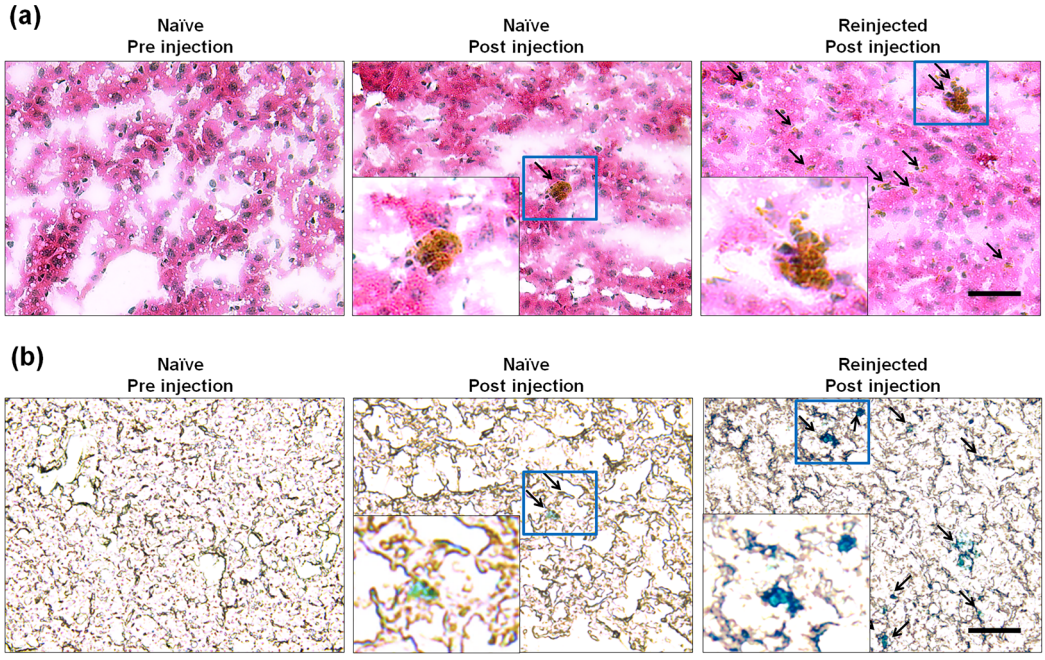

Figure 8. H&E and Prussian blue (PB) staining of liver tissue sections. (a) H&E staining of the liver tissues revealed no cells with nanoparticle accumulation from the preinjected naïve group. Minimal nanoparticle presence was found in the liver sections from the naïve group after receiving an injection of nanoparticles. Liver sections from the reinjected mice showed high cellular uptake of nanoparticles. Black arrows indicate the presence of nanoparticles within the cell. (b) PB staining validated the findings from H&E, showing no iron contents in preinjected naïve mice and high nanoparticle accumulation in the naïve group after nanoparticle injection and in reinjected mice.

***Ex Vivo* Biodistribution Study.** Ex vivo biodistribution was used to validate the finding of quantitative PET analysis. At Day 10 postsurgery, nanoparticle accumulation in the liver of the reinjected group was significantly higher than the naïve group. In contrast, uptake of the nanoparticle in the other organs of the naïve group was higher than those of the reinjected group, including the blood pool and ischemic hindlimb. The long circulation half-life of RGO-IONP-PEG in the naïve group could attribute to the higher passive targeting of nanoparticles to ischemic hindlimb and nonspecific uptakes in the other organs. There was no significant difference between the biodistribution values of the stomach, intestine, skin, and brain (Figure 5a). At Day 17 postsurgery, liver uptake was significantly higher in the reinjected group, while the naïve group displayed nanoparticle localization in circulation, ischemic hindlimb, bone, and lungs (Figure 5b).

Anti-PEG IgM ELISA. Anti-PEG IgM is the most well-known mediator of the ABC phenomenon.[28] We measured

DOI: 10.1021/acsami.6b05840
ACS Appl. Mater. Interfaces 2016, 8, 17955−17963

anti-PEG IgM before injection and at 7 and 14 days postinjection of ^{64}Cu-RGO-IONP-PEG. Anti-PEG IgM was detectable in the serum of mice at Day 7 and 14 postinjection (Figure 6). Hence, the ABC phenomenon in the present study was also likely to be mediated by anti-PEG IgM, similar to the ABC effect elicited by other types of nanomaterials.

Photoacoustic (PA) Imaging. PA imaging was performed to confirm the accumulation RGO-IONP-PEG in the liver by detecting the intrinsic PA imaging properties of RGO. At 72 h postinjection of the nanoparticle, the naïve and reinjected mice both showed positive PA signal in the liver; yet the signal was much higher in the reinjected mice (Figure 7).

Histological Analysis. Histological examination tissue sections from the naïve and reinjected groups were used to further evaluate nanoparticle accumulation. H&E staining revealed that the nanoparticles accumulated in the Kupffer cells and other phagocytic cells of the liver in both naïve and reinjected groups, yet this accumulation was much higher in the reinjected group. Prussian blue (PB) is used to detect the presence of iron in tissues by the formation of $Fe_4(Fe[CN]_6)_3$, which produces a bright cyan color.[29] Using the PB stain for detecting IONPs, we found enhanced signal in the liver of the reinjected group, while the naïve group showed little IONP accumulation (Figure 8). From these findings, it can be deduced that that the ABC phenomenon increases the amount of nanoparticles sequestered by the liver.

The most compelling mechanism of the ABC phenomenon is the anti-PEG immunoglobulin M (IgM) and complement activation-mediated clearance of PEGylated nanomaterials.[16] Specifically, the immune system produces anti-PEG IgM in response to an injection of exogenous PEGylated nanomaterials. When an animal is re-exposed to the PEGylated materials, the reinjected nanomaterials are quickly recognized by the anti-PEG IgM. In return, this process results in complement activation and removal of the nanomaterials by the mononuclear phagocytic system (MPS). In the present study, we found a positive correlation between anti-PEG IgM and increased liver accumulation of nanoparticles, which resulted from the ABC effect.

The ABC phenomenon has been reported in multiple studies using lipid-based or polymeric nanocarriers. In the previous studies, the nanocarriers were labeled with radioisotopes or small molecules because they do not have their own signal. Dam et al. used *N*-hydroxysuccinimidyl hydrazino nicotinate hydrochloride−distearoylphosphatidylethanolamine (HYNIC-DSPE) as a chelator for radiolabeling of liposomes.[30] In addition, Ishida et al. labeled liposomes with ^{3}H-cholesteryl hexadecyl ether (^{3}H−CHE).[14] Alternatively, Wang et al. employed tocopheryl nicotinate (TN) as an indicator by including TN during the formation of lipid-based nanocarriers.[27] Therefore, it was challenging to conclude whether the whole nanocarriers or just a labeled subunit was affected by the ABC phenomenon. In the present study, we confirmed that the ABC phenomenon induced hepatic clearance of the nanoparticle, which was validated by PA signal from RGO and iron content from IONP. Furthermore, there is no accurate way to confirm the existence of lipid-based or polymeric nanoparticles in the tissue; hence, to the best of our knowledge, the present study is the first report providing histological evidence demonstrating the enhanced accumulation of organic−inorganic hybrid nanoparticles in liver tissue as induced by the ABC phenomenon. While our previous study demonstrated that RGO-IONPs display minimal toxicity in healthy tissues,[20] some studies have shown that RGO may induce intracellular reactive oxygen species.[31] Despite its preclinical use for drug delivery and diagnostic imaging,[32] its low excretability, potential toxicity, and potential interaction with serum proteins have limited the clinical translation of this nanoplatform.

The present study is the first report demonstrating the ABC phenomenon using organic−inorganic hybrid nanoparticles. As multiple types of hybrid nanoparticles display excellent theranostic properties that may allow for clinical translation, deeper insight into the ABC phenomenon is essential for advancing these nanoplatforms to the clinic. In particular, the IONP/polymer nanoparticle exhibits a great potential for temperature-responsive drug delivery in various disease models.[33] Also, hybrid quantum dot-liposome nanoparticles have shown minimal toxicity and excellent tumor uptake in cancer models.[34] Hence, the observation of the ABC phenomenon with RGO-IONP-PEG may provide valuable insight into the development and clinical translation of other hybrid nanoparticles.

CONCLUSIONS

This study further confirms that the ABC phenomenon occurs after reinjection of PEGylated nanoparticles, including ^{64}Cu-RGO-IONP-PEG. This is the first report showing that PEGylated organic−inorganic hybrid nanoparticles can elicit the ABC phenomenon in mice. This process can effectively limit the passive targeting capabilities of nanomaterials to accumulate in ischemic tissues, such as peripheral arterial disease, which was assessed using a murine model of hindlimb ischemia. Furthermore, we could show that the nanoparticles were cleared to the liver due to the phenomenon. This observation may be valuable information which should be considered during developing targeted imaging and/or drug delivery probes using the long circulating PEGylated nanoparticles.

ASSOCIATED CONTENT

Supporting Information

The Supporting Information is available free of charge on the ACS Publications website at DOI: 10.1021/acsami.6b05840.

Characterization of the nanomaterials and quantitative uptake determined by positron emission tomography (PET) imaging (PDF)

AUTHOR INFORMATION

Corresponding Author

*E-mail: wcai@uwhealth.org. Phone: 608-262-1749. Fax: 608-265-0614.

Author Contributions

#These authors contributed equally to this work

Notes

The authors declare no competing financial interest.

ACKNOWLEDGMENTS

This work was supported, in part, by the University of Wisconsin—Madison, the National Institutes of Health (NIBIB/NCI 1R01CA169365, 1R01EB021336, P30CA014520, T32GM08349, T32CA009206, and S10-OD018505), the National Science Foundation (DGE-

DOI: 10.1021/acsami.6b05840
ACS Appl. Mater. Interfaces 2016, 8, 17955−17963

1256259), and the American Cancer Society (125246-RSG-13-099-01-CCE).

ABBREVIATIONS

PAD	peripheral arterial disease
ABC	accelerated blood clearance
PEG	polyethylene glycol
CLI	critical limb ischemia
AFM	atomic force microscopy
IONP	iron oxide nanoparticles
MRI	magnetic resonance imaging
PET	positron emission tomography
RGO	reduced graphene oxide
% ID/g	percent injected dose per gram of tissue

REFERENCES

(1) American Diabetes, A Peripheral Arterial Disease in People with Diabetes. *Diabetes Care* **2003**, *26*, 3333−3341. 10.2337/diacare.26.12.3333

(2) Criqui, M. H.; Aboyans, V. Epidemiology of Peripheral Artery Disease. *Circ. Res.* **2015**, *116*, 1509−1526.

(3) Samolsky Dekel, B. G.; Melotti, R. M.; Gargiulo, M.; Freyrie, A.; Stella, A.; Di Nino, G. Pain Management in Peripheral Arterial Obstructive Disease: Oral Slow-Release Oxycodone Versus Epidural L-Bupivacaine. *Eur. J. Vasc. Endovasc. Surg.* **2010**, *39*, 774−778.

(4) Varu, V. N.; Hogg, M. E.; Kibbe, M. R. Critical Limb Ischemia. *J. Vasc. Surg.* **2010**, *51*, 230−241.

(5) Berger, J. S.; Hiatt, W. R. Medical Therapy in Peripheral Artery Disease. *Circulation* **2012**, *126*, 491−500.

(6) Dormandy, J.; Heeck, L.; Vig, S. The Fate of Patients with Critical Leg Ischemia. *Semin. Vasc. Surg.* **1999**, *12*, 142−147.

(7) Tongers, J.; Roncalli, J. G.; Losordo, D. W. Therapeutic Angiogenesis for Critical Limb Ischemia: Microvascular Therapies Coming of Age. *Circulation* **2008**, *118*, 9−16.

(8) Amsden, B. G. Delivery Approaches for Angiogenic Growth Factors in the Treatment of Ischemic Conditions. *Expert Opin. Drug Delivery* **2011**, *8*, 873−890.

(9) Violi, F.; Basili, S.; Berger, J. S.; Hiatt, W. R. Antiplatelet Therapy in Peripheral Artery Disease. *Handb. Exp. Pharmacol.* **2012**, *210*, 547−563.

(10) Tu, C.; Das, S.; Baker, A. B.; Zoldan, J.; Suggs, L. J. Nanoscale Strategies: Treatment for Peripheral Vascular Disease and Critical Limb Ischemia. *ACS Nano* **2015**, *9*, 3436−3452.

(11) Xu, C.; Shi, S.; Feng, L.; Chen, F.; Graves, S. A.; Ehlerding, E. B.; Goel, S.; Sun, H.; England, C. G.; Nickles, R. J.; Liu, Z.; Wang, T.; Cai, W. Long Circulating Reduced Graphene Oxide-Iron Oxide Nanoparticles for Efficient Tumor Targeting and Multimodality Imaging. *Nanoscale* **2016**, *8*, 12683.

(12) Yang, K.; Feng, L.; Hong, H.; Cai, W.; Liu, Z. Preparation and Functionalization of Graphene Nanocomposites for Biomedical Applications. *Nat. Protoc.* **2013**, *8*, 2392−2403.

(13) Ishida, T.; Kiwada, H. Accelerated Blood Clearance (ABC) Phenomenon Upon Repeated Injection of Pegylated Liposomes. *Int. J. Pharm.* **2008**, *354*, 56−62.

(14) Ishida, T.; Harada, M.; Wang, X. Y.; Ichihara, M.; Irimura, K.; Kiwada, H. Accelerated Blood Clearance of Pegylated Liposomes Following Preceding Liposome Injection: Effects of Lipid Dose and Peg Surface-Density and Chain Length of the First-Dose Liposomes. *J. Controlled Release* **2005**, *105*, 305−317.

(15) Koide, H.; Asai, T.; Hatanaka, K.; Urakami, T.; Ishii, T.; Kenjo, E.; Nishihara, M.; Yokoyama, M.; Ishida, T.; Kiwada, H.; Oku, N. Particle Size-Dependent Triggering of Accelerated Blood Clearance Phenomenon. *Int. J. Pharm.* **2008**, *362*, 197−200.

(16) Saadati, R.; Dadashzadeh, S.; Abbasian, Z.; Soleimanjahi, H. Accelerated Blood Clearance of Pegylated PLGA Nanoparticles Following Repeated Injections: Effects of Polymer Dose, Peg Coating, and Encapsulated Anticancer Drug. *Pharm. Res.* **2013**, *30*, 985−995.

(17) Abu Lila, A. S.; Kiwada, H.; Ishida, T. The Accelerated Blood Clearance (ABC) Phenomenon: Clinical Challenge and Approaches to Manage. *J. Controlled Release* **2013**, *172*, 38−47.

(18) Jokerst, J. V.; Lobovkina, T.; Zare, R. N.; Gambhir, S. S. Nanoparticle Pegylation for Imaging and Therapy. *Nanomedicine (London, U. K.)* **2011**, *6*, 715−728.

(19) England, C. G.; Im, H. J.; Feng, L.; Chen, F.; Graves, S. A.; Hernandez, R.; Orbay, H.; Xu, C.; Cho, S. Y.; Nickles, R. J.; Liu, Z.; Lee, D. S.; Cai, W. Re-assessing the Enhanced Permeability and Retention Effect in Peripheral Arterial Disease Using Radiolabeled Long Circulating Nanoparticles. *Biomaterials* **2016**, *100*, 101−109.

(20) Yang, K.; Hu, L.; Ma, X.; Ye, S.; Cheng, L.; Shi, X.; Li, C.; Li, Y.; Liu, Z. Multimodal Imaging Guided Photothermal Therapy Using Functionalized Graphene Nanosheets Anchored with Magnetic Nanoparticles. *Adv. Mater.* **2012**, *24*, 1868−1872.

(21) Orbay, H.; Hong, H.; Zhang, Y.; Cai, W. PET/SPECT Imaging of Hindlimb Ischemia: Focusing on Angiogenesis and Blood Flow. *Angiogenesis* **2013**, *16*, 279−287.

(22) Shi, S.; Orbay, H.; Yang, Y.; Graves, S. A.; Nayak, T. R.; Hong, H.; Hernandez, R.; Luo, H.; Goel, S.; Theuer, C. P.; Nickles, R. J.; Cai, W. PET Imaging of Abdominal Aortic Aneurysm with ^{64}Cu-Labeled Anti-CD105 Antibody Fab Fragment. *J. Nucl. Med.* **2015**, *56*, 927−932.

(23) Yang, Y.; Hernandez, R.; Rao, J.; Yin, L.; Qu, Y.; Wu, J.; England, C. G.; Graves, S. A.; Lewis, C. M.; Wang, P.; Meyerand, M. E.; Nickles, R. J.; Bian, X. W.; Cai, W. Targeting CD146 with a ^{64}Cu-labeled Antibody Enables in Vivo Immunopet Imaging of High-Grade Gliomas. *Proc. Natl. Acad. Sci. U. S. A.* **2015**, *112*, E6525−6534.

(24) Yang, X. Y.; Zhang, X. Y.; Ma, Y. F.; Huang, Y.; Wang, Y. S.; Chen, Y. S. Superparamagnetic Graphene Oxide-Fe3O4 Nanoparticles Hybrid for Controlled Targeted Drug Carriers. *J. Mater. Chem.* **2009**, *19*, 2710−2714.

(25) Slovut, D. P.; Lipsitz, E. C. Surgical Technique and Peripheral Artery Disease. *Circulation* **2012**, *126*, 1127−1138.

(26) Kim, J.; Cao, L.; Shvartsman, D.; Silva, E. A.; Mooney, D. J. Targeted Delivery of Nanoparticles to Ischemic Muscle for Imaging and Therapeutic Angiogenesis. *Nano Lett.* **2011**, *11*, 694−700.

(27) Wang, C.; Cheng, X.; Su, Y.; Pei, Y.; Song, Y.; Jiao, J.; Huang, Z.; Ma, Y.; Dong, Y.; Yao, Y.; Fan, J.; Ta, H.; Liu, X.; Xu, H.; Deng, Y. Accelerated Blood Clearance Phenomenon Upon Cross-Administration of Pegylated Nanocarriers in Beagle Dogs. *Int. J. Nanomed.* **2015**, *10*, 3533−3545.

(28) Hashimoto, Y.; Shimizu, T.; Abu Lila, A. S.; Ishida, T.; Kiwada, H. Relationship between the Concentration of Anti-Polyethylene Glycol (PEG) Immunoglobulin M (IgM) and the Intensity of the Accelerated Blood Clearance (ABC) Phenomenon against Pegylated Liposomes in Mice. *Biol. Pharm. Bull.* **2015**, *38*, 417−424.

(29) Schlorf, T.; Meincke, M.; Kossel, E.; Gluer, C. C.; Jansen, O.; Mentlein, R. Biological Properties of Iron Oxide Nanoparticles for Cellular and Molecular Magnetic Resonance Imaging. *Int. J. Mol. Sci.* **2011**, *12*, 12−23.

(30) Dams, E. T.; Laverman, P.; Oyen, W. J.; Storm, G.; Scherphof, G. L.; van Der Meer, J. W.; Corstens, F. H.; Boerman, O. C. Accelerated Blood Clearance and Altered Biodistribution of Repeated Injections of Sterically Stabilized Liposomes. *J. Pharmacol. Exp. Ther.* **2000**, *292*, 1071−1079.

(31) Dutta, T.; Sarkar, R.; Pakhira, B.; Ghosh, S.; Sarkar, R.; Barui, A.; Sarkar, S. Ros Generation by Reduced Graphene Oxide (RGO) Induced by Visible Light Showing Antibacterial Activity: Comparison with Graphene Oxide (GO). *RSC Adv.* **2015**, *5*, 80192−80195.

(32) Yang, K.; Feng, L.; Hong, H.; Cai, W.; Liu, Z. Preparation and Functionalization of Graphene Nanocomposites for Biomedical Applications. *Nat. Protoc.* **2013**, *8*, 2392−2403.

(33) Vivero-Escoto, J. L.; Huang, Y. T. Inorganic-Organic Hybrid Nanomaterials for Therapeutic and Diagnostic Imaging Applications. *Int. J. Mol. Sci.* **2011**, *12*, 3888−3927.

(34) Al-Jamal, W. T.; Al-Jamal, K. T.; Bomans, P. H.; Frederik, P. M.; Kostarelos, K. Functionalized-Quantum-Dot-Liposome Hybrids as Multimodal Nanoparticles for Cancer. *Small* **2008**, *4*, 1406−1415.

DOI: 10.1021/acsami.6b05840
ACS Appl. Mater. Interfaces 2016, 8, 17955−17963